Microscopic Validation of Macroscopic *In Vivo* Images Enabled by Same-Slide Optical and Nuclear Fusion

Kazumasa Inoue, Ph.D.[1,2], Summer Gibbs, Ph.D.[1], Fangbing Liu, Ph.D.[1]
Jeong Heon Lee, B.S.[1], Yang (Allison) Xie, B.S.[1], Yoshitomo Ashitate, M.D.[1],
Hirofumi Fujii, M.D., Ph.D.[3], John V. Frangioni, M.D., Ph.D.[1,4,5], and Hak Soo Choi, Ph.D.[1,*]

[1] Department of Medicine and [4] Department of Radiology,
Beth Israel Deaconess Medical Center and Harvard Medical School, Boston, MA 02215, USA
[2] Department of Radiological Sciences, Tokyo Metropolitan University, Tokyo 116-8551, Japan
[3] Functional Imaging Division, Research Center for Innovative Oncology,
National Cancer Center Hospital East, Kashiwa 277-8577, Japan
[5] Current address: Curadel, LLC, 377 Plantation Street, Worcester, MA 01605, USA

First author: Kazumasa Inoue, Ph.D.
BIDMC, Room SL-B10
330 Brookline Avenue, Boston, MA 02215
TEL: 617-667-7329, FAX: 617-667-0981
Email: kinoue@bidmc.harvard.edu

[*] Correspondence to: Hak Soo Choi, Ph.D.
BIDMC, Room SL-436A
330 Brookline Avenue, Boston, MA 02215
TEL: 617-667-0692, FAX: 617-667-0981
Email: hchoi@bidmc.harvard.edu

Financial Support: This work was funded by NIH grant #R01-CA-134493, #R01-EB-010022 and #R01-EB-01152, and a grant from the Tuberous Sclerosis Alliance.

Word Count: 4435 (5000 limit)

Running Head: Microscopic optical/nuclear validation

ABSTRACT

It is currently difficult to determine the molecular and cellular basis for radioscintigraphic signals obtained during macroscopic *in vivo* imaging. The field is in need of technology that helps bridge the macroscopic and microscopic regimes. To solve this problem, we developed a fiducial marker (FM) simultaneously compatible with 2-color near-infrared (NIR) fluorescence (700 and 800 nm), autoradiography (ARG), as well as conventional hematoxylin and eosin (H&E) histology.

Methods: The FM was constructed from an optimized concentration of commercially available human serum albumin (HSA), 700 nm and 800 nm NIR fluorophores, ^{99m}Tc-pertechnatete, DMSO, and glutaraldehyde (GA). Lymphangioleiomyomatosis (LAM) cells co-expressing the sodium iodide symporter (NIS) and green fluorescent protein (GFP) were labeled with 700 nm fluorophore and ^{99m}Tc-pertechnatete, then administered intratracheally into CD-1 mice. After *in vivo* SPECT imaging, and *ex vivo* SPECT and NIR fluorescence imaging of the lungs, 30 μm frozen sections were prepared and processed for 800 nm NIR fluorophore co-staining, ARG, and H&E staining on the same slide using the FMs to co-register all data sets.

Results: Optimized FMs, composed of 100 μM unlabeled HSA, 1 μM NIR fluorescent HSA, 15% DMSO, and 3% GA in PBS (pH 7.4) were prepared within 15 min, displayed homogeneity and stability, and were visible by all imaging modalities, including H&E staining. Using these FMs, tissue displaying high signal by SPECT could be dissected and analyzed on the same slide and at the microscopic level for 700 nm NIR fluorescence, 800 nm NIR fluorescence, ARG, and H&E histopathological staining.

Conclusion: When multimodal FMs are combined with a new technique for simultaneous same-slide NIR fluorescence imaging, ARG, and H&E staining, macroscopic *in vivo* images can now be studied unambiguously at the microscopic level.

Word Count: 284 (350 limit)

Keywords: Molecular and cellular basis of signal, Multimodality imaging; Fiducial marker; Autoradiography; NIR fluorescence; H&E staining

INTRODUCTION

The development of new clinical radiotracers for single-photon emission computed tomography (SPECT) and positron emission tomography (PET) is of critical importance (*1,2*). However, validating that the signal obtained during *in vivo* radioscintigraphic imaging is emanating from the target of interest can be a challenge (*3-5*). Particularly difficult is the validation of signals at the cellular and/or molecular level.

Clinically, histopathological staining with hematoxylin and eosin (H&E) is the gold standard for identification of specific cells and tissues (*6*), however, ambiguity is common. To ensure proper identification, one or more immunomarkers is typically employed, and precipitating pigments are used in conjunction with H&E to label cells of interest (*3,7*). The problem with conventional immunohistochemistry, however, is that the H&E image itself is masked by the precipitating pigments (*8*). To solve this problem, our group has previously developed a technology to perform two independent wavelengths of near-infrared (NIR) fluorescence immunostaining on the same specimen, and the same slide, as conventional H&E (Gibbs et al., manuscript in review). Thus, the unadulterated H&E can be used in conjunction with immunomarkers to unambiguously identify cells and/or molecules of interest.

What is needed in the field of nuclear medicine is the ability to correlate radioscintigraphic signals measured using macroscopic *in vivo* imaging techniques with validation performed at the single cell level. But, few such techniques exist. For this reason, we focused the present study on developing an optimized fiducial marker (FM) that permits acquisition and co-registration of H&E, NIR fluorescence, and autoradiography (ARG) data sets, on the same specimen, and on same slide. We hypothesized that such a technology would enable unambiguous validation of macroscopic nuclear images at the microscopic level.

MATERIALS AND METHODS

Reagents: Cy5.5 NHS ester was purchased from GE Healthcare (Piscataway, NJ), and ZW800-1 was synthesized as previously reported (*9*). They were diluted to 10 mM in DMSO and stored at -80 ºC under reduced light conditions. Human serum albumin (HSA) and glutaraldehyde (GA) were purchased from Sigma (St. Louis, MO) and Electron Microscopy Sciences (Hatfield, PA), respectively. ^{99m}Tc-pertechnatete was purchased from Cardinal Health (Dublin, OH). The red blood cell labeling kit (Ultra Tag® RBC) was purchased from Covidien (Hazelwood, MO). Rabbit polyclonal anti-GFP antibody was purchased from Abcam (Cambridge, MA). Magnesium chloride and trypsin-versene were purchased from Fisher Scientific (Pittsburgh, PA) and Cambrex (Walkersville, MD), respectively.

Preparation of HSA700 and HSA800: All steps were performed under reduced light conditions. HSA suspended in PBS pH 7.8 was first purified using gel filtration chromatography (GFC) with a Bio-Gel P-6 desalting column (Bio-Rad, Hercules, CA) to remove small molecules that interfere with covalent conjugation by NHS esters. Two equivalents of Cy5.5 NHS ester or ZW800-1 NHS ester was added to the purified HSA in PBS, pH 7.8 and incubated for 3 h to form a stable amide linkage. HSA700 and HSA800 were purified using GFC as above, and the labeling ratio was calculated from the ratio of extinction coefficients between the HSA (ε_{280} nm = 32,900 $M^{-1}cm^{-1}$) and the NIR fluorophore (Cy5.5, ε_{700} nm = 250,000 $M^{-1}cm^{-1}$; ZW800-1, ε_{770} nm = 249,000 $M^{-1}cm^{-1}$). The final NIR fluorophore labeling ratios for HSA700 and HSA800 were 0.95 and 0.96, respectively. The optical spectra of HSA700 and HSA800 were obtained with a UV-Visible and fluorescence spectrophotometer (Varian, Santa Clara, CA). Final products were stored as 0.2 mM stock solutions in PBS, pH 7.4 at 4 ºC.

Optimization of the Multimodality Fiducial Marker: Unlabeled HSA, HSA700, HSA800, ^{99m}Tc-pertechnatete, DMSO, and GA concentrations were varied systematically, and the homogeneity and stability of conjugation to an amine-coated Superfrost® Plus (VWR, Bridgeport, NJ) microscope slide was measured. Reagents were vortexed together gently at room temperature (RT) and 0.2 μL of the solution spotted by hand onto the glass slide. The FM was then incubated for 15 min at RT, washed with distilled water, and dried for 15 min at RT. The glass slide was exposed to a phosphorimaging screen overnight at -20 °C and the screen read

using a Typhoon™ 9400 system (GE Healthcare). The pixel size and depth were set to 25 μm and 16-bits, respectively. Phosphorimaging screen was erased for a minimum of 2 h before the next experiment and confirmed to be back to baseline.

Multichannel Fluorescence Microscope: HSA700 and HSA800 were imaged on a Nikon TE 300 microscope system equipped with mercury and xenon excitation sources (Chiu Technical Corporation, Kings Park, NY) and an Orca-ER 12-bit camera (Hamamatsu, Bridgewater, NJ). To obtain fluorescence images of HSA700, the xenon light source was passed through a 650/45-nm BP excitation filter and a 700/35-nm BP emission filter (Chroma Technology, Brattleboro, VT). To obtain fluorescence images of HSA800, the xenon light source was passed through a 750/50-nm BP excitation filter and an 810/40-nm BP emission filter (Chroma). Slides were then H&E stained using a standard clinical protocol. The signal intensity, homogeneity, and shape of all obtained fluorescence images were compared before and after H&E staining.

Labeling and Imaging of LAM cells: LAM 621-327 cells (*10*) were cultured in a 50/50 mixture of DMEM/F12 (Invitrogen, Carlsbad, CA) supplemented with epidermal growth factor (EGF, 10 ng/ml; Sigma-Aldrich, St. Louis, MO), 200-nM hydrocortisone (Sigma-Aldrich), 25-μg/ml insulin (Sigma-Aldrich), 50-nM sodium selenite (Sigma-Aldrich), 10-μg/ml transferrin (Sigma-Aldrich), 1.6-μM ferrous sulfate (Sigma-Aldrich), and 15% fetal bovine serum (Gemini). LAM cells were grown at approximately 70% confluence on a 10-cm diameter tissue culture plate and washed once with PBS containing 1-mM $MgCl_2$. LAM cells were labeled with 2-μM Cy5.5 NHS ester in 10 mL PBS/$MgCl_2$ for 30 min at 37°C, washed 3 times, and 10% of the components of the Ultra Tag RBC labeling kit was added. LAM cells were mixed by gently inverting the components of the RBC kit for 10 min at 37 °C then 37 MBq (1 mCi) of ^{99m}Tc-pertechnetate was added to the plate. After gentle rocking for 2 h at 37 °C, cells were washed once with buffer and trypsinized by adding 2 mL trypsin-versene (Sigma-Aldrich). LAM cells labeled with Cy5.5 and ^{99m}Tc were then washed 3 times by centrifuging at 2000 rpm for 5 min. The supernatant was discarded carefully, so as not to disturb the cell pellet. The LAM cells were resuspended in 200-μL PBS/$MgCl_2$ and loaded on the microscope glass slide for ARG scanning. ARG was performed using the same parameters as described above. The signal of GFP was then imaged

using a fluorescence microscope equipped with a 480/40-nm BP excitation filter and a 535/50-nm BP emission filter.

Immunofluorescence staining: ZW800-1 conjugated donkey (Dk) anti-rabbit (Rb) secondary antibody was prepared as follows: 400 μL of Dk antibody (stock concentration = 1.2 mg/mL) was buffer exchanged with PBS using spin columns (Vivaspin 500, 10 kDa MWCO, GE Healthcare) to eliminate any sodium azide that might be present in the stock solution. The buffer exchange was performed using centrifugation at 8000 rpm 5 times, 3 min each. The antibody solution was adjusted to pH 8 and 5-25 equivalents of ZW800-1 NHS ester was added. After 3-h reaction at RT, the NIR-antibody conjugate was purified using GFC as described above. Purified fractions were collected and concentrated to 50 μL volume by centrifugation at 10,000 rpm for 3 min. The labeling ratio, calculated from the ratio of extinction coefficients for the antibody ($\varepsilon_{280\ nm}$ = 150,000 $M^{-1}cm^{-1}$) and ZW800-1 ($\varepsilon_{770\ nm}$ = 249,000 $M^{-1}cm^{-1}$), was 1.5. PBS containing 2.5% goat serum was added to the slide and incubated for 1 h at RT to block nonspecific protein binding sites. Then, the Rb polyclonal anti-GFP antibody (1:100 dilution in PBS + 0.1% bovine serum albumin + 0.1% Tween 20) was added and incubated overnight at RT. After washing 3 times with PBS containing 0.5% Tween 20 (PBS/T), 5-μM ZW800-1 conjugated secondary antibody was added and incubated for 2 h at RT. After incubation, the LAM cells were washed with PBS/T 3 times, 5 min each time. LAM cells were then fixed in 2% paraformaldehyde in PBS for 15 min at RT, and then stained with H&E. After H&E staining, color imaging and 800 nm anti-GFP immunofluorescence imaging were performed.

***In Vivo* and *Ex Vivo* Imaging:** Animals used in this study were housed in an Association for Assessment and Accreditation of Laboratory Animal Care (AAALAC)-certified facility, staffed by full-time veterinarians. Animal studies were performed under the supervision of Beth Israel Deaconess Medical Center's Institutional Animal Care and Use Committee (IACUC) in accordance with approved institutional protocol #155-2008. CD-1 mice of either sex, 8 to 10 weeks in age were purchased from Charles River Laboratories (Wilmington, MA). Mice were anesthetized with 100-mg/kg ketamine and 10-mg/kg xylazine (Webster Veterinary, Fort Devens, MA) intraperitoneally. 18G gavage tubing (Fine Science Tool, Foster, CA) was placed in the trachea and 10 x 10^6 LAM cells labeled with Cy5.5 and ^{99m}Tc in 150-μL PBS/$MgCl_2$

administered intratracheally. After 15 min, the mice underwent euthanasia, and a thoracotomy procedure was performed to enucleate the lung tissues.

SPECT and CT images were acquired using a NanoSPECT/CT® scanner (Bioscan, Inc., Washington. D.C., USA) equipped has 4 NaI(Tl) detectors. For SPECT imaging, 9-pinhole apertures with a diameter of 1.4 mm were used on each detector. The energy window was set at 140 keV ± 20%. SPECT imaging was performed at 24 projections/rotation and 300 s/projection. The projected data were reconstructed using HiSPECT® software (Scivis, Göttingen, Germany) and a dedicated ordered-subsets expectation-maximization (OSEM) algorithm employing multiplexed Multi-Pinhole SPECT technology. Voxel size and Gaussian filter size (full width at half maximum; FWHM) were set at 0.3 mm and 1.9 mm, respectively. The iterative update number (subset × iteration) was 27. A CT scan was performed at 45 kVp, 177 μA, 240 projections/rotation using a CMOS detector with a 96-μm pixel size. Projected data were reconstructed by setting the voxel size to 100 μm.

After *in vivo* SPECT/CT imaging, the lung tissue was excised and imaged *ex vivo* using the same protocol. The 700-nm NIR fluorescence and color images were then imaged with the FLARE™ real-time intraoperative imaging system, as described in detail previously (*11,12*). Extracted lung tissues were placed in 2% paraformaldehyde in PBS for 30 min before mounting on the Tissue-Tek OCT (Sakura Finetek, Torrance, CA). The sample was frozen in liquid nitrogen and cryosectioned into a 30-μm thick section for fluorescence imaging, ARG, and H&E staining. Three FMs were placed around the tissue. After ARG scanning and H&E staining, anti-GFP antibody staining was performed using the optimized protocol as described above. The dual channel NIR fluorescence and color images were obtained using a Nikon 55i fluorescence microscope equipped with an encoded motorized stage (Prior Scientific). To obtain the 700-nm fluorescence image, the xenon lamp was passed through a 650/45-nm BP excitation filter, a 680-nm LP dichroic, and a 710/50-nm BP emission filter. For 800-nm fluorescence imaging, the xenon lamp was passed through a 750/50-nm BP excitation filter, 810-nm LP dichroic, and an 824/47-nm BP emission filter. The obtained dual NIR fluorescence and ARG images were then merged with the H&E histology image based on the pre-positioned 3 FMs.

RESULTS

Optimization of the Fiducial Marker: The chemical structures and optical spectra of HSA700 and HSA800 are shown in Figure 1. Since the half-life of ^{99m}Tc is relatively short ($T_{1/2}$ = 6 h) and a stable chemical reaction is required, we used a simple and facile cross-linking reaction to conjugate albumin to the glass slide while simultaneously trapping ^{99m}Tc pertechnetate in the protein mesh (*27*). The type of slide most commonly used in clinical histopathology laboratories is the "plus" slide. The primary amines conjugated to the surface of the plus slide helps tissue adhere and also serves as the matrix for FM conjugation.

Preparing FMs that were perfectly homogeneous, however, proved to be a challenge. ^{99m}Tc-pertechnetate (0.37 KBq/μL; 0.01 μCi/μL), unlabeled HSA (100 μM), HSA700 (1 μM), and HSA800 (1 μM) were fixed in PBS, pH 7.4, at several different concentrations of GA (1%, 3%, and 5%) and with different concentrations of DMSO (0%, 5%, 10%, and 15%) for 15 min at RT. The NIR fluorescence signal of HSA700 and HSA800 were imaged before and after H&E staining to ensure that the FM was stable. In all conditions tested, the signal intensity and shape of FMs were not altered significantly by H&E staining, and the FM was visible by brightfield microscopy (Figure 2). However, homogeneity of the FMs was improved by increasing the concentrations of GA and DMSO. Optimized conditions for FM production were found to be 100 μM unlabeled HSA, 1 μM HSA700, 1 μM HSA800, 0.01 μCi/μL (0.37 KBq/μL) ^{99m}Tc pertechnetate, 3% GA, and 15% DMSO in PBS (pH 7.4) for 15 min at RT.

Cell Labeling and Imaging: To create single cells that were NIR fluorescent at 700 nm and 800 nm, as well as radioactive, LAM cells stably co-expressing NIS and GFP were incubated with ^{99m}Tc-pertechnetate and 700 nm Cy5.5 NHS (Figure 1). After fixation, GFP was detected using an unlabeled primary antibody and an 800 nm NIR fluorescent secondary antibody (Figure 3B). Although expression of NIS alone is sufficient to accumulate ^{99m}Tc-pertechnetate into a cell (*13,14*), we found that incubation with Sn^{2+}, which diffuses across the cell membrane, accumulates intracellularly, and reduces Tc^{7+}, helped to retain the radioisotope.

The inherent differences in sensitivity, specificity, and resolution among microscopic NIR fluorescence imaging, ARG, and H&E staining are shown in Figure 3C. In particular, currently available phosphorimaging cassettes are not designed for high-energy isotopes,

resulting in significant blurring of what would otherwise be single cell resolution of the ARG signal.

Microscopic Analysis of Macroscopic Radioscintigraphic Images: 700 nm NIR fluorescent and radioactive LAM cells were administered intratracheally into CD-1 mice (Figure 4A) and *in vivo* SPECT/CT imaging was performed (Figure 4B). After surgical removal of the lung, SPECT/CT, color, and 700-nm fluorescence images were obtained (Figure 4B) and a portion of lung tissue having both optical and nuclear signal was excised and processed as described in Materials and Methods. As shown in Figure 4C, it was possible to analyze 2 independent channels (700 nm and 800 nm) of NIR fluorescence, as well as ARG, on the same specimen, on the same slide, with all data sets able to be co-registered using the FMs. Both NIR fluorescent and H&S optical imaging could be performed with single cell resolution (Figure 4D). As might be expected based on the experimental protocol, LAM cells were found to be distributed peri-bronchially (Figure 4D).

DISCUSSION

This study addressed a fundamental problem in the field of nuclear medicine, the validation of macroscopic radioscintigraphic signals at the microscopic level. Having already optimized two channels of NIR fluorescence microscopy with H&E staining on the same slide (Gibbs et al., manuscript in review), we assumed that adding the ARG data set would be straightforward. On the contrary, co-registration of data sets between optical and nuclear imaging was found to be a major issue because ARG lacks identifiable landmarks and was acquired the night before the optical images. Even if a dual-functional diagnostic agent (i.e., SPECT/NIR fluorescent probe) is utilized, a similar problem has been reported (*15*).

To circumvent this issue, we describe a simple, inexpensive, FM that can be applied to a standard "plus" slide and permits rotation, translation, and morphing of data sets as needed among brightfield microscopy, NIR fluorescence immunomicroscopy, and ARG. This FM can be created with commercially available reagents in only 15 min, which is an important point when considering the short half-life of many SPECT and PET radiotracers.

The biological example we show in this study, namely the tracking of LAM cells after administration into the airspaces of the lung, actually has important implications. Our group recently described a new animal model of LAM and the related disease tuberous sclerosis complex (TSC) that recapitulates the homing of LAM/TSC cells to virtually every lymph node basin in the body (*10*). However, it is extremely difficult to study the mechanism of cellular translocation and lymph node homing because the process involves single cells. Armed with the technology described in this paper, it should now be possible to track cells using *in vivo* imaging methods and to analyze the source of measured signals at the microscopic level. This same strategy could be used to study similar processes, such as the early steps of cancer metastasis.

Nevertheless, our study also has limitations. The resolution of conventional ARG using phosphorimaging is inadequate. Currently available phosphorimaging plates are not designed for high-energy gamma radioisotopes, and significant blurring of resolution occurs (see, for example, Figure 4C). Estimates of full-width at half-maximum (FWHM) resolution for ^{99m}Tc and ^{18}F are 350 μm and 460 μm, respectively (*16*). Fortunately, the development of high-resolution ARG systems is an active area of investigation (*17-19*) and it is hoped that such systems will become commercially available in the near future.

CONCLUSION

We developed a specialized FM and processing techniques that permitted same-slide ARG, 700-nm and 800-nm NIR fluorescence, and H&E histopathological analysis at the single cell level. FM marker preparation took only 15 min using readily available reagents. Using this technology, macroscopic nuclear images can be validated at the microscopic level.

ACKNOWLEDGMENTS

We thank David Burrington, Jr. for editing and Eugenia Trabucchi for administrative assistance. This study was supported by the following grants from the National Institutes of Health: NCI grant #R01-CA-134493 (JVF), NIBIB grant #R01-EB-010022 (JVF and HSC), and NIBIB grant #R01-EB-011523 (HSC and JVF), and a grant from the Tuberous Sclerosis Alliance. The views expressed are solely those of the authors and do not necessarily reflect those of the National Institutes of Health.

DISCLOSURES

John V. Frangioni, M.D., Ph.D.: Dr. Frangioni is currently CEO of Curadel, LLC, a for-profit company which has licensed FLARE™ technology, including the adrenal gland-specific NIR fluorophores described in this study, from Beth Israel Deaconess Medical Center.

REFERENCES

1. Patil V, Gada K, Panwar R, et al. Imaging small human prostate cancer xenografts after pretargeting with bispecific bombesin-antibody complexes and targeting with high specific radioactivity labeled polymer-drug conjugates. *Eur J Nucl Med Mol Imaging*. 2012.

2. Wuest M, Trayner BJ, Grant TN, et al. Radiopharmacological evaluation of 6-deoxy-6-[18F]fluoro-D-fructose as a radiotracer for PET imaging of GLUT5 in breast cancer. *Nucl Med Biol*. 2011;38:461-475.

3. Abasolo I, Pujal J, Rabanal RM, et al. FDG PET imaging of Ela1-myc mice reveals major biological differences between pancreatic acinar and ductal tumours. *Eur J Nucl Med Mol Imaging*. 2009;36:1156-1166.

4. Muller C, Forrer F, Schibli R, Krenning EP, de Jong M. SPECT study of folate receptor-positive malignant and normal tissues in mice using a novel 99mTc-radiofolate. *J Nucl Med*. 2008;49:310-317.

5. Oka S, Hattori R, Kurosaki F, et al. A preliminary study of anti-1-amino-3-18F-fluorocyclobutyl-1-carboxylic acid for the detection of prostate cancer. *J Nucl Med*. 2007;48:46-55.

6. Ankle MR, Joshi PS. A study to evaluate the efficacy of xylene-free hematoxylin and eosin staining procedure as compared to the conventional hematoxylin and eosin staining: An experimental study. *J Oral Maxillofac Pathol*. 2011;15:161-167.

7. De Saint-Hubert M, Prinsen K, Mortelmans L, Verbruggen A, Mottaghy FM. Molecular imaging of cell death. *Methods*. 2009;48:178-187.

8. Valencia JC, Pacheco-Rodriguez G, Carmona AK, et al. Tissue-specific renin-angiotensin system in pulmonary lymphangioleiomyomatosis. *Am J Respir Cell Mol Biol*. 2006;35:40-47.

9. Choi HS, Nasr K, Alyabyev S, et al. Synthesis and in vivo fate of zwitterionic near-infrared fluorophores. *Angew Chem Int Ed Engl*. 2011;50:6258-6263.

10. Liu F, Lunsford EP, Tong J, et al. Real-time monitoring of tumorigenesis, dissemination, and drug response in a preclinical model of lymphangioleiomyomatosis/tuberous sclerosis complex. *PLoS ONE*. 2012;In Press.

11. Tanaka E, Choi HS, Fujii H, Bawendi MG, Frangioni JV. Image-guided oncologic surgery using invisible light: completed pre-clinical development for sentinel lymph node mapping. *Ann Surg Oncol*. 2006;13:1671-1681.

12. Troyan SL, Kianzad V, Gibbs-Strauss SL, et al. The FLARE intraoperative near-infrared fluorescence imaging system: a first-in-human clinical trial in breast cancer sentinel lymph node mapping. *Ann Surg Oncol*. 2009;16:2943-2952.

13. Bengel FM, Schachinger V, Dimmeler S. Cell-based therapies and imaging in cardiology. *Eur J Nucl Med Mol Imaging*. 2005;32 Suppl 2:S404-416.

14. Seo JH, Jeon YH, Lee YJ, et al. Trafficking macrophage migration using reporter gene imaging with human sodium iodide symporter in animal models of inflammation. *J Nucl Med*. 2010;51:1637-1643.

15. Zhang R, Lu W, Wen X, et al. Annexin A5-conjugated polymeric micelles for dual SPECT and optical detection of apoptosis. *J Nucl Med*. 2011;52:958-964.

16. Knol RJ, de Bruin K, de Jong J, van Eck-Smit BL, Booij J. In vitro and ex vivo storage phosphor imaging of short-living radioisotopes. *J Neurosci Methods*. 2008;168:341-357.

17. Chen L, Gobar LS, Knowles NG, Liu Z, Gmitro AF, Barrett HH. Direct imaging of radionuclide-produced electrons and positrons with an ultrathin phosphor. *J Nucl Med*. 2008;49:1141-1145.

18. Chen L, Gobar LS, Knowles NG, Wilson DW, Barrett HH. Direct Charged-Particle Imaging System Using an Ultra-Thin Phosphor: Physical Characterization and Dynamic Applications. *IEEE Trans Nucl Sci*. 2009;56:2628-2635.

19. Russo P, Lauria A, Mettivier G, et al. 18F-FDG positron autoradiography with a particle counting silicon pixel detector. *Phys Med Biol*. 2008;53:6227-6243.

FIGURE LEGENDS

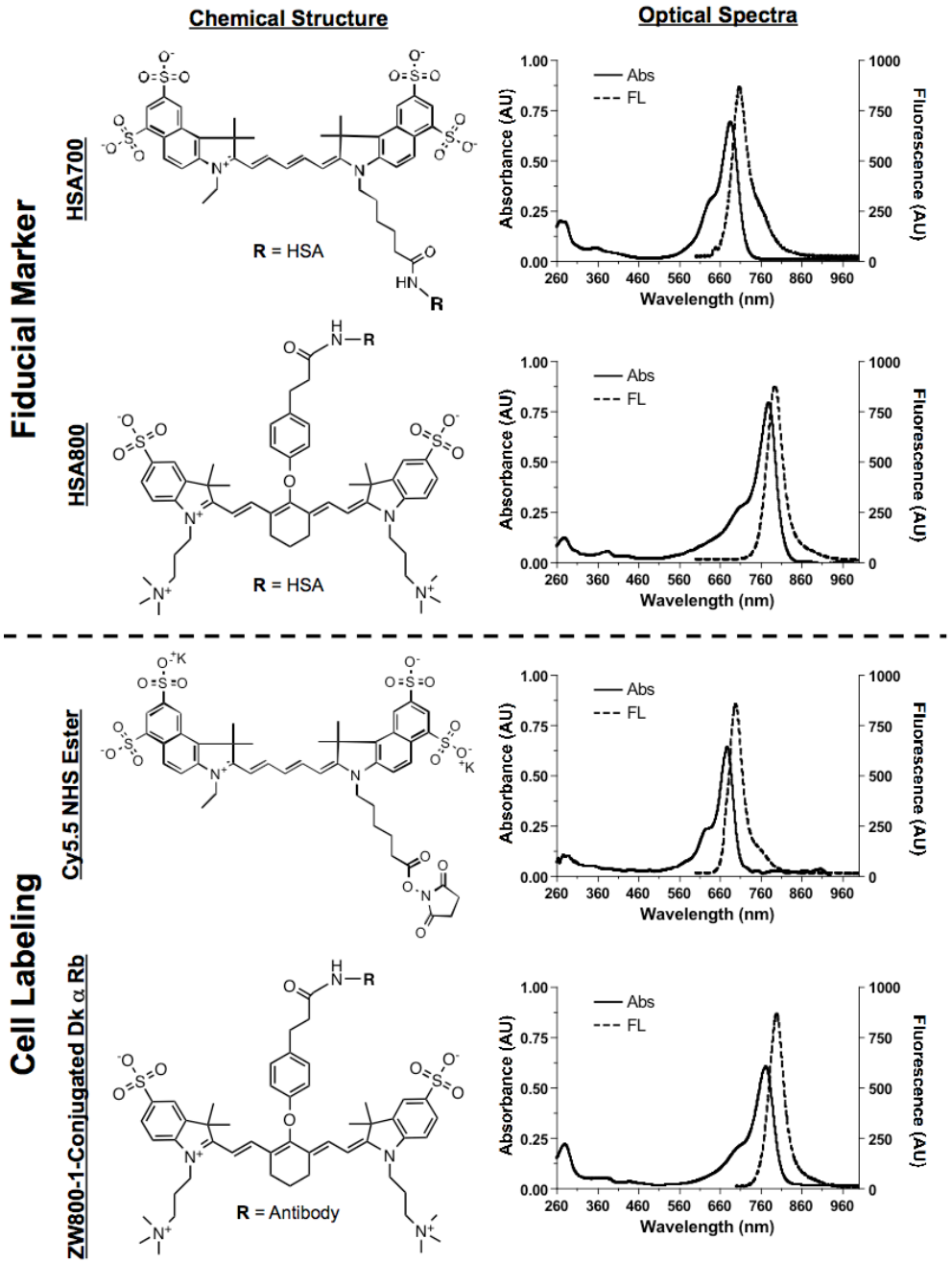

Figure 1 – Chemical structure and optical spectra of fiducial markers and cell labeling reagents: HSA700 and HSA800 for fiducial markers were prepared by conjugating Cy5.5 and ZW800-1, respectively to purified human serum albumin (HSA). Cell labeling was performed using Cy5.5 NHS ester (700 nm fluorophore) and ZW800-1-conjugated donkey anti-rabbit (Dk α Rb) antibody. Shown are chemical structures (left) and optical spectra (right).

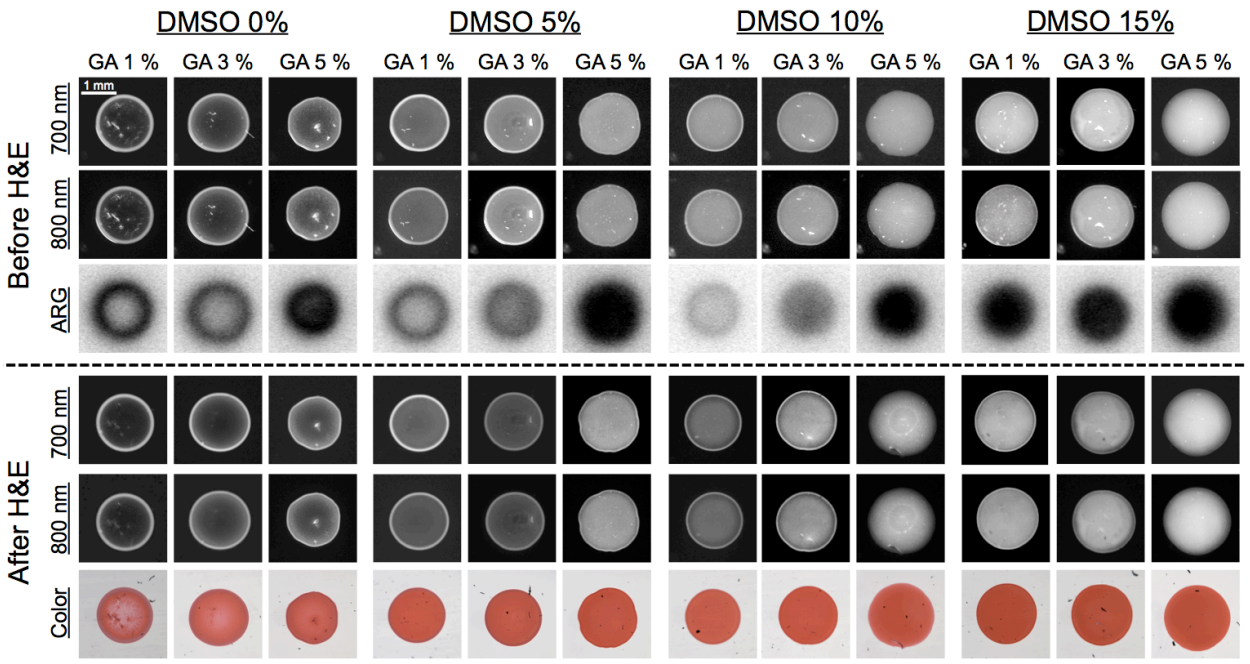

Figure 2 – Optimization of fiducial markers: Unlabeled HSA (100 μM), HSA700 (1 μM), HSA800 (1 μM), and ^{99m}Tc-pertechnetate (0.01 μCi/μL; 0.37 KBq/μL) in PBS, pH 7.4 were fixed while the concentrations of GA and DMSO were systematically varied as shown. NIR fluorescence signal intensity was measured before (top) and after (bottom) H&E staining. ARG was measured before H&E staining only. All NIR fluorescence images have identical exposure times and normalizations. Data are representative of n = 3 independent experiments.

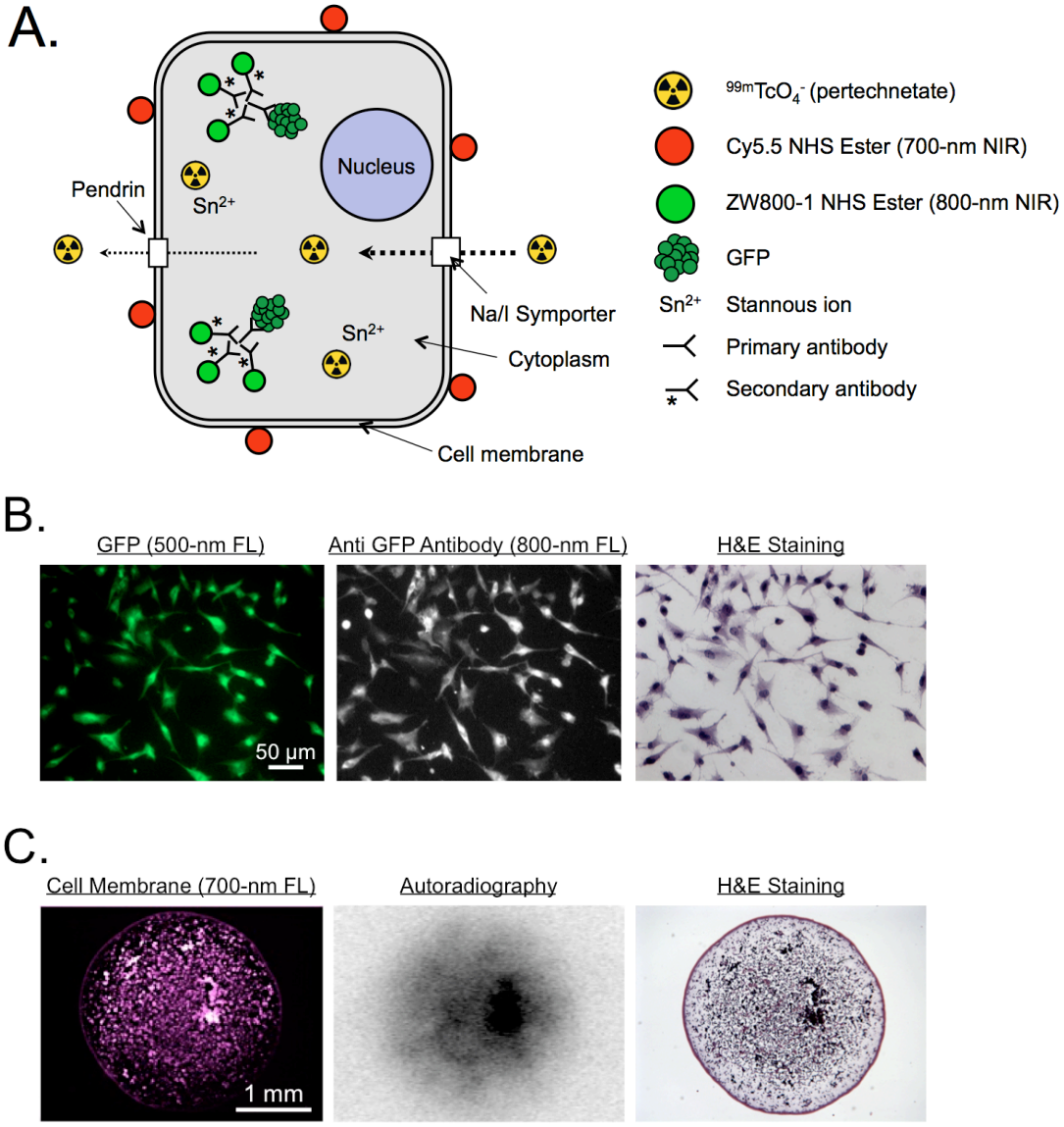

Figure 3 – Multimodality labeling of single cells:

A. Summary of the various NIR fluorescent and radioactive molecules used to label LAM cells. Cy5.5 NHS ester (700-nm NIR) was conjugated to the cell membrane. ZW800-1 (800-nm NIR) conjugated secondary antibody was used for immunofluorescence staining of GFP. ^{99m}Tc-pertachnetate was accumulated via NIS, while stannous ion (Sn^{2+}) was used to improve retention of the radioisotope in the cell.

B. Immunofluorescence staining of GFP. Rabbit polyclonal anti-GFP antibody and ZW800-1 conjugated donkey anti-rabbit secondary antibody staining of LAM cells expressing GFP. The 500-nm fluorescence signal for GFP was imaged before H&E staining, while 800-nm fluorescence and color microscopy was performed after H&E staining.

C. Multimodality microscopy of LAM cells. Shown are the 700-nm fluorescence image, autoradiography (ARG), and H&E color image for a 4 mm diameter spot of LAM cells on a glass slide. Note single cell resolution by NIR fluorescence and H&E.

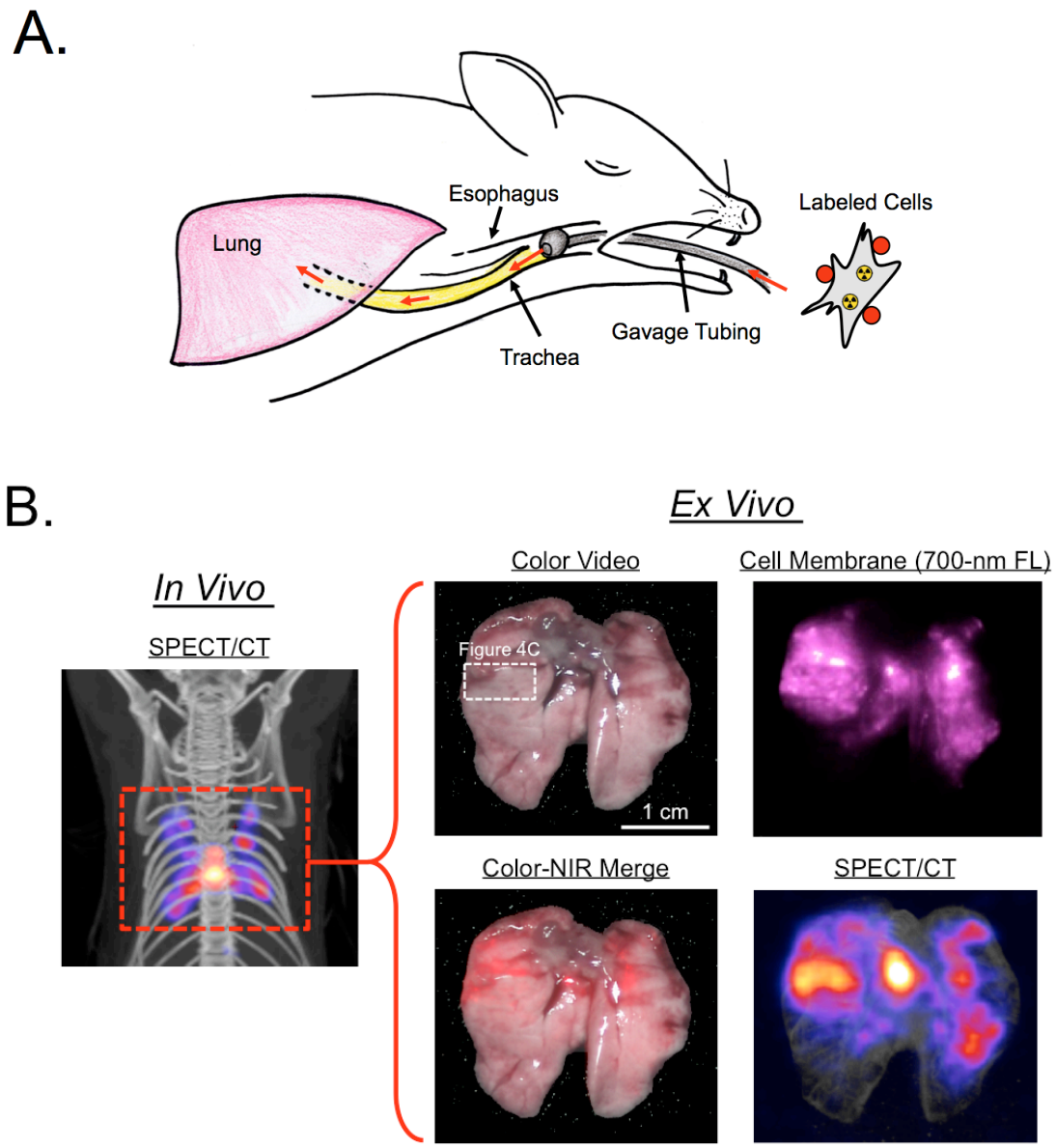

Figure 4 – *In vivo* and *ex vivo* multifunctional imaging:

A. Schematic representation of the *in vivo* mouse model. Labeled LAM cells (see Figure 3A) were administered intratracheally into CD-1 mice using gavage tubing.

B. *In vivo* maximal intensity projection (MIP) SPECT/CT image (left) and *ex vivo* color, 700-nm fluorescence, color-NIR merge (700 nm signal is pseudo-colored in red) and MIP SPECT/CT images (right) of the excised lung. Images shown are representative of n = 3 independent experiments. The dashed white rectangle delineates the excised tissue sample studied in Figure 4C.

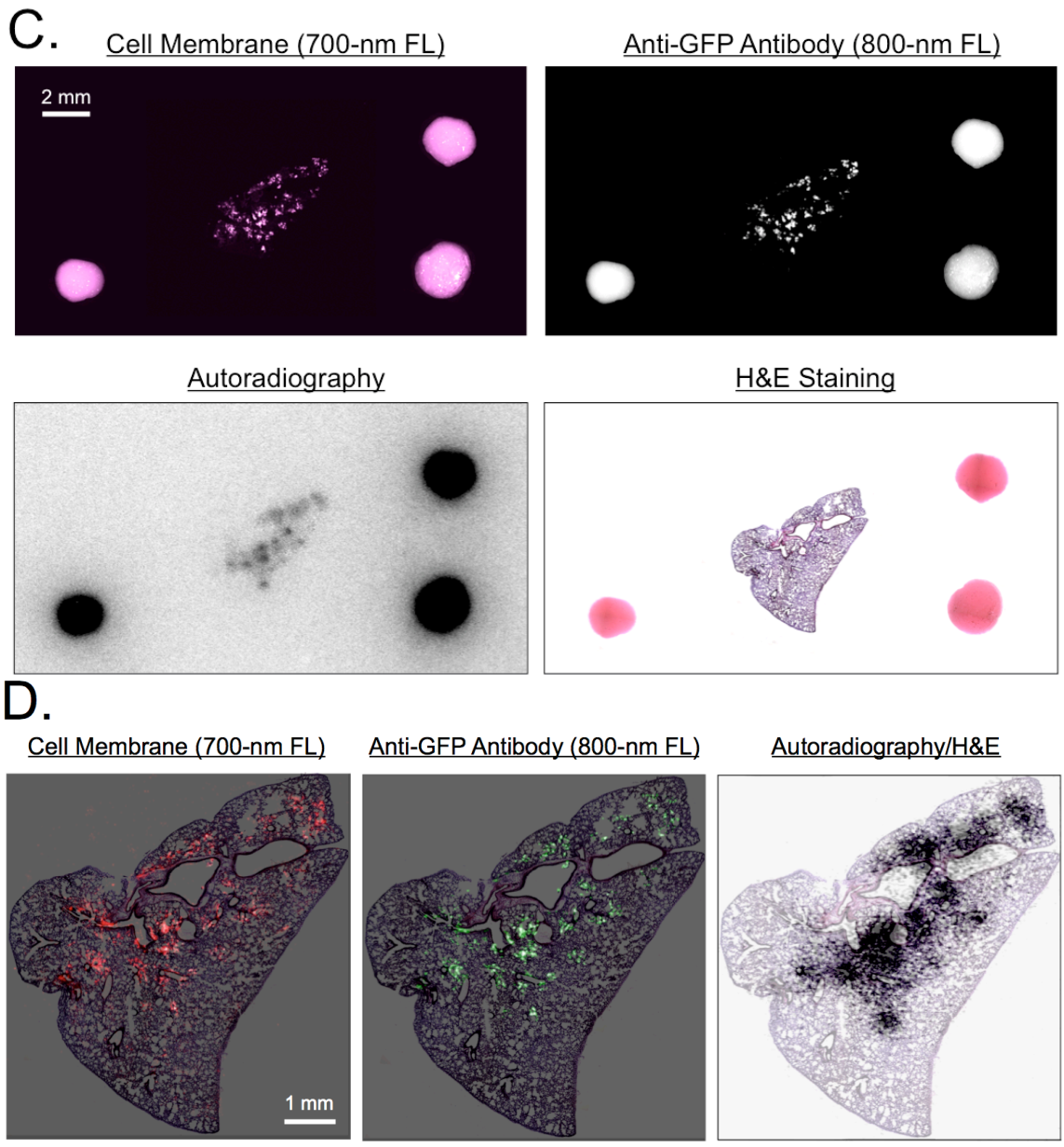

Figure 4 – *In vivo* and *ex vivo* multifunctional imaging (Continued):

C. Same-slide 700 nm NIR fluorescence (cell membrane staining), 800 nm NIR fluorescence (anti-GFP staining), ARG, and H&E staining of LAM cells in the lung tissue of a CD-1 mouse. 2 mm diameter multimodal FMs visible in each image were used to co-register the data sets.

D. Same as (C) but at higher magnification, with the 700 nm NIR fluorescent signal pseudo-colored in red, the 800 nm NIR fluorescent signal pseudo-colored in green, and the ARG signal superimposed on the H&E image.